Design consideration of micro thin film solid-oxide fuel cells

INSTITUTE OF PHYSICS PUBLISHING JOURNAL OF MICROMECHANICS AND MICROENGINEERING

J. Micromech. Microeng. **15** (2005) S185–S192 doi:10.1088/0960-1317/15/9/S03

Design consideration of micro thin film solid-oxide fuel cells

Yanghua Tang, Kevin Stanley, Jonathan Wu, Dave Ghosh and Jiujun Zhang

Institute for Fuel Cell Innovation, National Research Council, 3250 East Mall, Vancouver, BC, Canada

E-mail: yanghua.tang@nrc-cnrc.gc.ca

Received 25 February 2005, in final form 21 June 2005
Published 15 August 2005
Online at stacks.iop.org/JMM/15/S185

Abstract

Miniaturized planar solid-oxide fuel cells (SOFCs) and stacks can be fabricated by thin film deposition and micromachining. Serious thermal stresses, originating in fabrication and during operation, cause thermal–mechanical instability of the constituent thin films. In this paper, the effect of thin film geometry on thermal stress and mechanical stability is evaluated to optimize the structure of a thin film. A novel design of thin circular electrolyte films for SOFCs is presented by using corrugated structures, with which small thermal stresses and a broad design range of structure parameters can be obtained. Thermal transfer analysis shows that heat loss by solid conduction is serious in thin films with a small radius. But thermal convection and radiation dominate heat loss in large thin films with a radius of several millimetres. Scale-dependent thermal characteristics show the importance of film size and packaging in optimization of thermal isolation for micro SOFCs. A novel flip-flop stack configuration for micro SOFCs is presented. This configuration allows multiple cells to share one reaction chamber, helps to obtain uniform flow fields, and simplifies the flow field network for micro fuel cell stacks.

1. Introduction

The capacity of conventional batteries cannot meet the power consumption requirements for increasing performance and functions of electronic products. SOFCs are drawing interest due to their high generation efficiency. Micro SOFCs are one possible choice for portable applications [1, 2]. The architecture of a solid-oxide fuel cell consists of a porous anode and cathode, separated by a dense solid-oxide electrolyte [3]. The traditional SOFC operates at high temperature where the electrolyte has sufficient ionic conductivity. Since the ionic resistance of the electrolyte decreases with its thickness, the performance can be improved by using thinner electrolyte. Conventional fabrication of SOFCs is based on bulk ceramic powder processes, such as tape casting and screen-printing, which do not lend themselves to thin film deposition. With the development of micromachining technology, it is possible to make dense and thin ceramic films with chemical and physical vapour deposition. A schematic of a micro planar SOFC with circular thin films is shown in figure 1.

Although thin film SOFCs have the advantage of low operating temperature (300–600 °C), the size of the thin laminated films is limited by the large thermal stresses originating in fabrication and during operation. Optimization of thin film structures is required to reduce thermal stress, increase the thin film area and improve the single cell performance. Heat loss is a serious problem in micro SOFCs because of the large ratio of surface to volume. It is important to improve the power efficiency by decreasing heat loss. Due to the low voltage of the single cell, micro SOFC stacks are needed in most applications. Microfabrication based on lithographic methods is suitable for making planar SOFC stacks. Conventional SOFC stacks are built in back-to-back orientation. A complicated bonding process is needed to build the multi-layer structure for this kind of planar micro SOFC stacks. Another configuration of SOFC stacks is to arrange the cell array in side-by-side orientation. All cells are fabricated on one wafer and connected to form a stack. However, a large planar network of flow fields is needed and leads to non-uniform reactant distribution [4].

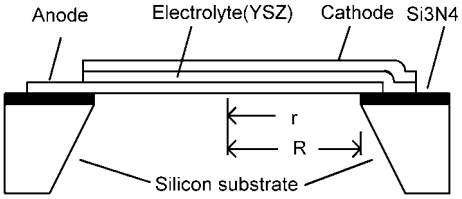

Figure 1. A schematic diagram of a thin film SOFC on silicon substrate.

Performance and reliability of micro SOFCs is scale dependent on its structure because of the properties of thermal mechanics and transfer in microstructures. In this paper, thermal stress and thermal transfer were analysed as a function of dimension in flat and corrugated circular films, leading to the optimization of the structure of micro SOFCs. A configuration of micro SOFCs is presented to form the stack on one wafer.

2. Thermal–mechanical reliability of electrolyte thin films

Layered thin films under thermal loading exhibit several failure modes: buckling, crazing, fracture and spalling. Investigation of all failure modes in the layered thin films complicates the design process. Moreover, the key to micro thin film SOFCs is to design a reliable and dense electrolyte film that can be self-supported. In the first analysis, a single circular electrolyte membrane is considered. The total stress of the microfabricated membrane is the sum of thermal stress, intrinsic stress and external stress. Intrinsic stress can be reduced by modifying the fabrication process parameters and materials. Thermal stress, which is seriously affected by film structures, is analysed in this section for the primary structure design. It is assumed that the film material is yttria-stabilized zirconia (YSZ) and the substrate is silicon.

2.1. Mechanics of thin films

For a flat isotropic film with thermal expansion coefficient α and radius R, the radial displacement under temperature difference ΔT between the film and environment is $\alpha R \Delta T$ without any constraint at the membrane edge. If the flat film is clamped, radial thermal stress σ_f limits the displacement.

$$\sigma_f = -\frac{\Delta\alpha E \Delta T}{1-\nu} \tag{1}$$

where E, ν and $\Delta\alpha$ are Young's modulus, the Poisson ratio of the film and the thermal expansion difference between the film and its substrate respectively. E, ν and the thermal expansion of a YSZ film are 200 GPa, 0.2 and 10×10^{-6} K^{-1} respectively [5]. Thermal expansion difference between the YSZ film and silicon is 7×10^{-6} K^{-1}. Negative values of σ_f denote compressive stress. Thermal stresses are uniform in the clamped flat circular film and independent of the geometry parameters: film thickness h and radius R.

A corrugated film often used in micromachined sensors can reduce the structure stress by allowing the structure dimension to change to some degree. Figure 2 shows the structure of the corrugated membrane. The fundamental parameter of the corrugated membrane is the profile factor q, which describes the ratio of rigidity of the corrugation.

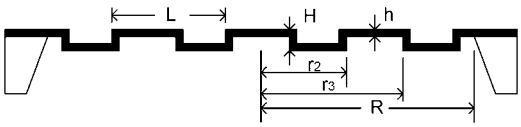

Figure 2. The meridian section of the corrugated membrane.

For shallow corrugations in which the ratio of the corrugation depth H to its wavelength L is less than 0.4, the profile factor q is given by [6]

$$q^2 = 1 + 1.5\frac{H^2}{h^2} \tag{2}$$

where q is in the range of 5 to 15 for most corrugated membranes. In special cases, it may be as high as 30. It is 1 for a flat membrane. The radial thermal stress σ_{cr} at radius r is given by [6]

$$\sigma_{cr} = -\frac{\Delta\alpha E \Delta T}{q}\left(\frac{r}{R}\right)^{q-1}. \tag{3}$$

Unlike a flat film, the radial thermal stress of the corrugated film is affected by geometry parameters and not uniform. The maximum thermal stress occurs at the film edge.

2.2. Failure criteria

The area of a thin electrolyte film in a micro solid-oxide fuel cell is an important factor in energy conversion and structure design. Larger area of an electrolyte film is helpful to obtain higher power output in a single cell and simplify the stack structure. But a large ceramic film increases the possibility of failure because large stresses reduce the reliability of a film. The film failure induced by stress is classified into several modes: spalling, fracture, crazing and buckling. These failure modes are affected by the stress state.

If the clamped film tends to expand due to temperature difference between the film and environment, compressive stress occurs. Sufficient compressive stress leads to film buckling. For a clamped flat membrane shown in figure 1, the critical stress σ_{fc} at which buckling occurs is given by [7]

$$\sigma_{fc} = -1.22\frac{E}{1-\nu^2}\left(\frac{h}{R}\right)^2. \tag{4}$$

It is shown that the absolute value of the critical stress is low for thin and large flat membranes ($h \ll R$).

Buckling of corrugated films occurs when sufficient radial load due to temperature differences between the membrane and outer rim is present. The critical stress σ_{cc} at which buckling happens is given by [8]

$$\sigma_{cc} = -\frac{E(q+1)^2}{48}\beta^2\left(\frac{h}{R}\right)^2 \tag{5}$$

where β is the buckling number dependent on q. For $q > 10$, β changes slightly from 4.8 to 5.14 [6]. For the corrugated film, it is possible to design large membranes and keep high critical stress by increasing the profile factor q. In other words, corrugation with a high ratio of H:h is advantageous.

To prevent thin films from buckling, the compressive thermal stress of a thin film should be smaller than its critical stress. By combining equations (1) and (4), temperature

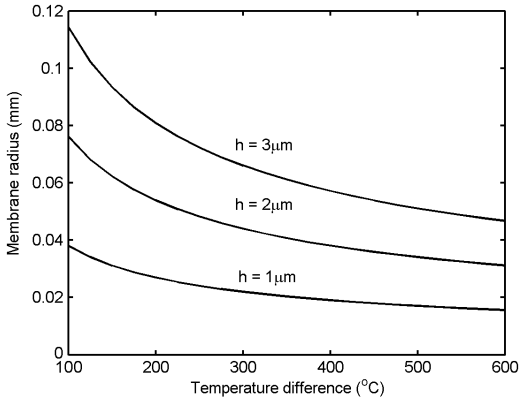

Figure 3. The maximum membrane radius versus temperature difference for a flat YSZ film.

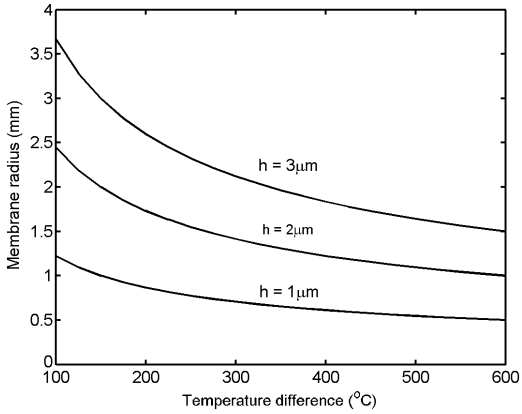

Figure 4. The maximum membrane radius versus temperature difference for a corrugated YSZ film (H:$h = 10$, $\beta = 5$).

difference ΔT as a function of limitation of the radius R of a flat thin film with the critical stress is given by

$$\Delta T = \frac{1.22}{(1+\nu)\Delta\alpha}\left(\frac{h}{R}\right)^2. \tag{6}$$

For a corrugated film, by combining equations (3) and (5), the relationship between the operation temperature difference and the film radius is expressed by

$$\Delta T = \frac{q(q+1)^2\beta^2}{48\Delta\alpha}\left(\frac{h}{R}\right)^2. \tag{7}$$

This equation shows that the profile factor q plays an important role in thermal–mechanical reliability of a corrugated thin film. Figures 3 and 4 show that the maximum radius of the corrugated membrane is substantially greater than that of the flat membrane. For a flat membrane of 1 μm thickness, the maximum of the radius is only 16 μm at $\Delta T = 600\ ^\circ$C, requiring a large array of cells to obtain sufficient power output. For the 1 μm thick corrugated film of $q = 12$, the maximum film radius is 500 μm at the same ΔT. Larger profile factor q can lead to a more than two orders of magnitude increase in cell area under the same temperature.

The main failure mode under the tensile stress is fractures by growth of cracks and flaws. The well-known Weibull statistics can be used to evaluate fracture failure. This failure model was expanded by Danzer [9] to incorporate the effects of volumes. For materials containing volume defects, the probability of failure is given by [9]

$$P = 1 - \exp\left[-\int_{V(\sigma>0)} n(\sigma)\,\mathrm{d}V\right] \tag{8}$$

where $n(\sigma)$ is a material function assumed to be independent of the position in the material and the direction of stress. It is given by

$$n(\sigma) = \frac{1}{V_0}\left(\frac{\sigma}{\sigma_0}\right)^m \tag{9}$$

where the Weibull modulus m and characteristic strength σ_0 are material parameters; m and σ_0 of YSZ are 6.7 and 236 MPa respectively [10]. V_0 is an arbitrary normalizing volume and often set to 1 mm^3. Thermal stress in a flat membrane is isotropic. By integrating $n(\sigma)$ on a flat circular membrane with radius R and thickness h, the failure probability P is given by

$$P = 1 - \exp\left[-\frac{2\pi}{V_0}\left(\frac{\sigma_f}{\sigma_0}\right)^m R^2 h\right]. \tag{10}$$

The failure probability of a flat film increases exponentially with the geometry parameter: R^2h. The maximum tensile stress σ_{ft} under failure possibility P is given by

$$\sigma_{ft} = \sigma_0\left[-\frac{V_0}{2\pi R^2 h}\ln(1-P)\right]^{1/m}. \tag{10'}$$

Thermal stress in a corrugated film is anisotropic. The tangential stress σ_{ctan} is given by [6]

$$\sigma_{\mathrm{ctan}} = -\Delta\alpha E \Delta T\left(\frac{r}{R}\right)^{q-1}. \tag{11}$$

Here $n(\sigma)$ is expressed as $n(\sigma_{cr}) + n(\sigma_{\mathrm{ctan}})$ in a corrugated membrane. By integrating $n(\sigma_{cr}) + n(\sigma_{\mathrm{ctan}})$ over the film volume V in equation (8), the possibility of failure in the rectangular corrugated film shown in figure 2 is given by

$$P = 1 - \exp\left[-\frac{2\pi}{V_0}(c_1 + c_2)\left(\frac{\sigma_{cm}}{\sigma_0}\right)^m\right] \tag{12}$$

where σ_{cm} is the maximum thermal stress in the corrugated membrane, and c_1 and c_2 are geometry parameters given by

$$c_1 = \left(1 + \frac{1}{q^m}\right)\frac{R^2 h}{m(q-1)+2} \tag{13}$$

$$c_2 = \left(1 + \frac{1}{q^m}\right) hH \sum_{i=1}^{2n} r_i \left(\frac{r_i}{R}\right)^{m(q-1)} \tag{14}$$

where n is the corrugation number and r_i is the radius of the corrugation, as shown in figure 2. c_1 is much greater than c_2 in a shallow corrugation (H/L<0.4). The failure probability P can be simplified by

$$P = 1 - \exp\left[-\frac{2\pi}{V_0}c_1\left(\frac{\sigma_{cm}}{\sigma_0}\right)^m\right]. \tag{15}$$

Here c_1 is less than the geometry factor R^2h in equation (10) by a factor of $m(q-1)+2$ $(1 + 1/q^m \approx 1)$. According to equations (10) and (15), it is concluded that the possibility of failure is lower in the corrugated film than that in the flat film at the same thermal stress. High values of q can reduce the

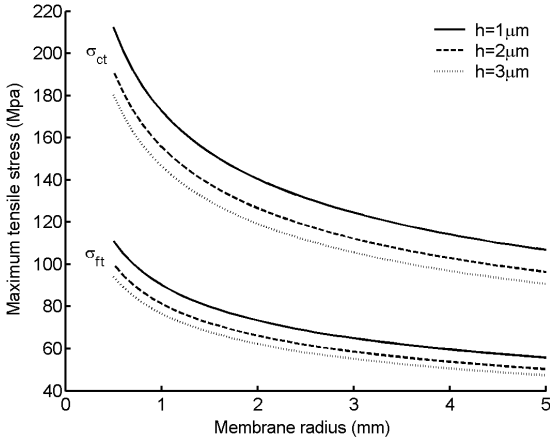

Figure 5. The maximum tensile stress of flat and corrugated membranes versus the membrane radius. (For the corrugated membrane, $n = 5$, $H{:}h = 10$.)

failure probability of a corrugated film. The maximum tensile stress σ_{ct} under failure possibility P is given by

$$\sigma_{ct} = \sigma_0 \left[-\frac{V_0}{2\pi c_1} \ln(1 - P) \right]^{1/m}. \qquad (15')$$

The critical stress as a function of film radius is plotted in figure 5 at a failure probability of 10^{-5}. It is shown that the critical stress in the corrugated film is almost twice as high as that in the flat film. In other words, YSZ films with a corrugated structure can withstand much higher tensile stress.

2.3. Design of film structures

The design map (figure 6) can be set up by equations (6), (7), (10) and (15) with Srikar's method [11]. The axes denote intrinsic stress and temperature difference. The limitation of temperature difference is $\Delta T \geqslant 0$. Compressive and tensile stresses are above and below the reference line $\sigma = 0$ respectively. Stress limitations for buckling and fracture are shown on the map. The design areas are formed in the grey triangles. Compared with the flat film, the corrugated film has lower thermal stress and higher critical stress. The design triangle of the corrugated film is bigger than that of the flat

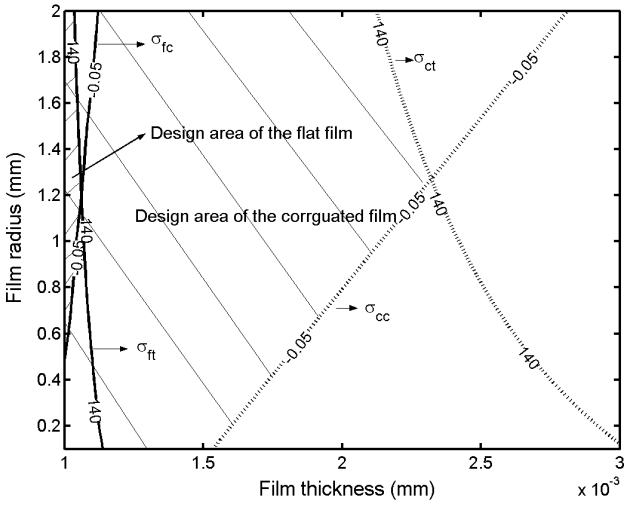

Figure 7. Design areas of corrugated films ($H{:}h = 10{:}1$) and flat films under the buckling critical stress of 0.05 MPa and the fracture critical stress of 140 MPa.

film. This design map shows that we can keep the film structure parameters R, h and increase the design area of corrugated films by bigger corrugated profile factor q. But for the flat film, the film radius and thickness have to be changed to increase its design area.

To compare design areas of corrugated and flat films, the design ranges of the film radius and thickness under designated stress limitation are expressed in figure 7. The corrugated profile factor q in this case is about 12. It is clear that the design area of the corrugated film is bigger by at least one order of magnitude than that of the flat film. By micromachining, corrugated supported membranes with a large profile factor q can be fabricated [12]. Because the buckling critical stress increases with q^2 in the corrugated film, its design area broadens quickly with q.

Thermal stress in the corrugated membrane increases with $(r/R)^{q-1}$ and thus is small in the middle of the film, as shown in figure 8. The value of tangential thermal stress at a radius of $0.7R$ occurs only by 1.4% of the maximum in the film with the profile factor of 12. The maximum thermal

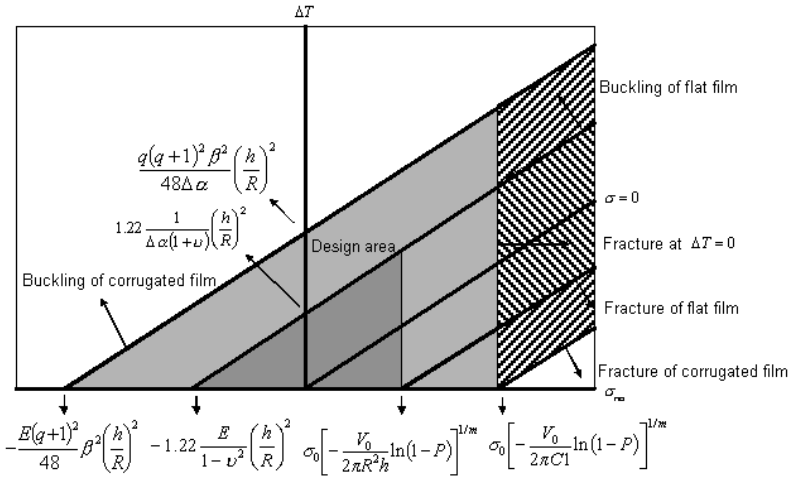

Figure 6. The design map for flat and corrugated films.

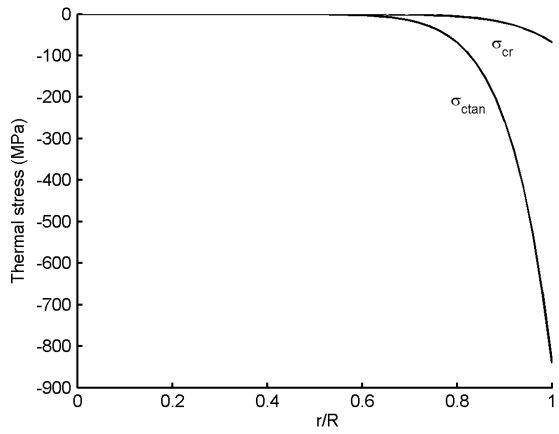

Figure 8. The radius and tangential thermal stress versus the relative membrane radius (H:h = 10:1, ΔT = 600 °C).

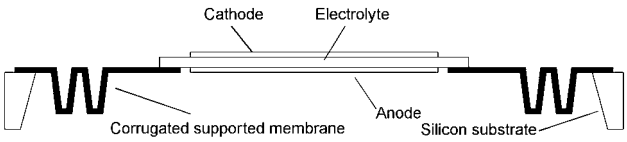

Figure 9. A flat thin electrolyte film mounted on a corrugated supporting membrane.

stress occurs at the corrugated film edge. The mechanical behaviour of the corrugated film can be described as a film with a clamped edge and free radial motion. The middle part of the corrugated membrane can expand due to less constraint and thus smaller stress occurs. By making full use of this characteristic, large, thin and flat YSZ films can be mounted on corrugated supported substrates to obtain a stable thermal–mechanical performance, as shown in figure 9. Flat thin films with corrugated edges can expand or contract under temperature variation to decrease stress. By micromachining, corrugated supported membranes with a large profile factor q can be fabricated to reduce the stress at the edge.

3. Heat loss in thin films

It is important to improve the performance of micro SOFCs by decreasing heat loss. There are three ways of heat loss in micro SOFCs: air convection, structure thermal conduction and radiation. Characteristics of heat loss in micro devices are scale dependent. To improve the efficiency of micro SOFCs, optimization of the micro SOFC structure and packaging is needed to decrease heat loss. Circular flat thin films are used in the following thermal analysis.

3.1. Heat loss in flat thin films

It is considered that a distributing heater is integrated on the film [13]. Uniform heat is assumed in this case, as shown in figure 10. It is also assumed that the support substrate is cooled and thus the boundary of the thin film has the low temperature T_b. In this condition, the temperature distribution in the flat film is given by [14]

$$T(r) = T_0 - (T_0 - T_b)\left(\frac{r}{R}\right)^2 \tag{16}$$

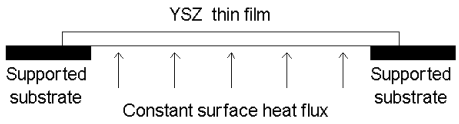

Figure 10. A schematic of the heated YSZ film.

where T_0 is the temperature in the centre of the thin film. The whole heat loss Q_h by thermal conduction is given by

$$Q_h = \pi k(T_0 - T_b)h, \tag{17}$$

where k is the thermal conductivity of the thin film. Heat loss by conduction changes linearly as a function of the thin film thickness h.

3.2. Heat loss by radiation

According to the Stefan–Boltzmann law, the heat flux q_e (W m^{-2}) emitted by a real surface is described by

$$q_e = \varepsilon\sigma T_S^4, \tag{18}$$

where ε is the emissivity of the surface, σ is the Stefan–Boltzmann constant (5.67 × 10^{-8} W m^{-2} K^{-4}), and T_S is the absolute temperature of the surface. It is assumed that the emissivity of YSZ is 0.4, which is equivalent to that of zirconia because they have a similar structure [15]. For a non-uniform temperature distribution in the circular thin film, the whole emissive power Q_e is given by

$$Q_e = \int_A \varepsilon\sigma T_S^4 \,\mathrm{d}A. \tag{19}$$

If the surface temperature distribution can be described by equation (16), the whole emitted power Q_e may be expressed as

$$Q_e = \frac{\varepsilon\sigma\pi R^2}{5}\left(T_0^4 + T_0^3T_b + T_0^2T_b^2 + T_0T_b^3 + T_b^4\right). \tag{20}$$

We conclude that heat loss by radiation increases with film area and is not affected by the thin film thickness. Low boundary temperature decreases the heat loss by radiation, which is opposite to the effect of thermal conduction.

3.3. Heat loss by natural air convection

A heated thin film in an air environment transfers heat into the surrounding air and causes natural convection of air in the vicinity. Heat loss q_a by convection is given by

$$q_a = \lambda\Delta T \tag{21}$$

where λ is the heat transfer coefficient. For a uniform heat flux, the average heat transfer coefficient $\bar{\lambda}$ is given by

$$\bar{\lambda} = \frac{\overline{Nu}\lambda}{L} \tag{22}$$

where L is the characteristic length, $9D/11$ for a circle plate with diameter D [16]. The pattern of natural airflow is important in convective thermal transfer. The Rayleigh number Ra, correlating the natural flow patterns, is a good indication of whether the natural convection boundary is laminar or turbulent. For the vertical plate, Ra at position x is given by

$$Ra = \frac{g\xi\Delta T x^3}{\nu\kappa}, \tag{23}$$

where g is gravity, ξ is the coefficient of thermal expansion of the fluid, ν is the kinematic viscosity of the fluid, and κ is the thermal diffusivity of the fluid.

Natural convection is laminar at Ra of less than 10^9. For air in the vertical plate of 10 mm diameter, the maximum of Ra is 4.46×10^4 ($g = 9.8$ m s^{-1}, $\xi = 3.22 \times 10^{-3}$ K^{-1}, $\nu = 16.94 \times 10^{-6}$ m^2 s^{-1}, $\kappa = 24.0 \times 10^{-6}$ m^2 s^{-1}, $\Delta T = 575$ K) [16]. It is assumed that the natural airflow near the heated thin film of micro SOFCs is laminar.

The average Nusselt number $\overline{Nu}$ is a non-dimensional parameter characterizing heat transfer. Larger Nusselt numbers express a better heat transfer performance. In the surface with a uniform heat flux, the average Nusselt number $\overline{Nu}$ is given by [16]

$$\overline{Nu} = 0.67 Ra_x^{1/4} f_2(Pr) \tag{24}$$

where the ΔT term in Ra_x is the temperature difference between the circular film centre and the environment. The function $f_2(Pr)$ of the Prandtl number Pr is given by [16]

$$f_2 = \left[1 + \left(\frac{0.437}{Pr}\right)^{9/16}\right]^{-4/9}. \tag{25}$$

The Prandtl number of air is 0.7 in this paper. The whole heat loss Q_a can be obtained by integrating equation (21) on the flat membrane surface:

$$Q_a = \int_s \bar{\lambda} \Delta T \, \mathrm{d}s. \tag{26}$$

If the surface temperature distribution can be described by equation (16), by combining equations (22)–(26), the heat loss Q_a by natural air convection in the thin film may be expressed as

$$Q_a = 1.27 \Delta T^{\frac{5}{4}} R^{\frac{7}{4}}. \tag{27}$$

The heat loss changes almost linearly with the thin film area and temperature difference between the thin film and environment.

3.4. Characteristics of thermal transfer in micro SOFCs

Figure 11 shows the plots of three kinds of heat losses as functions of temperature difference between the thin film and environment in a 3 μm thick film. To make meaningful comparison with heat loss by thermal conduction, heat loss by radiation and convection was drawn at the film radius of 0.7 mm and 0.9 mm. Plots show that heat loss by air convection exceeds that by film structure conduction in the thin film of over 0.7 mm radius at a temperature difference of more than 260 K. By increasing the film radius to 0.9 mm, heat loss by air convection dominates over the other two kinds of thermal transfer once the film temperature is higher than the environment temperature. At a temperature difference of 420 K, heat loss by radiation is bigger than that by structure conduction in the film of more than 0.9 mm radius. In other words, the percentage of heat loss by structure conduction decreases with a larger film radius. Figure 12 shows that

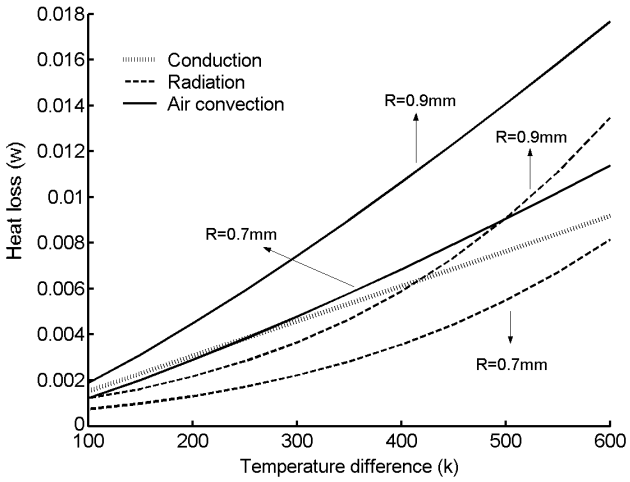

Figure 11. Heat loss versus temperature difference in a flat thin YSZ film with a less than 1 mm radius and 3 μm thickness ($T_b = 323$ K).

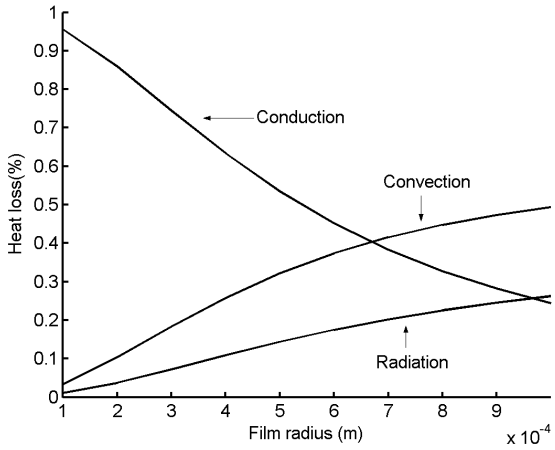

Figure 12. Heat loss versus film radius at the temperature difference of 350 K.

the percentage of heat loss by structure conduction decreases quickly with the film radius. Calculation shows that thermal conduction leads to only 10% of the whole heat loss in the film of 3 mm radius at a temperature difference of 300 K.

Heat loss can be reduced by optimization of film structures and packaging. Heat loss by thermal conduction decreases with smaller film thickness. But for large films, solid conduction contributes a small part to the whole heat loss. Therefore, the choice of film thickness is guided mainly by thermal–mechanical consideration.

Heat loss by natural convection through the ambient air can be reduced by suitable packaging, such as vacuum packaging [17]. The gas reactors in high operation temperature are enclosed in the vacuum cavity and connected with the outside by fluidic interconnects. But the thermal–mechanical reliability of vacuum packaging under high operation temperature should be dealt with. Heat loss by radiation increases with T^4 and R^2. It is the next most important source of heat loss for a large film and exceeds the heat loss by air convection at high operating temperature, as shown in figure 13. Reflective internal surface of the cell package that is formed by depositing a metal film can decrease radiation.

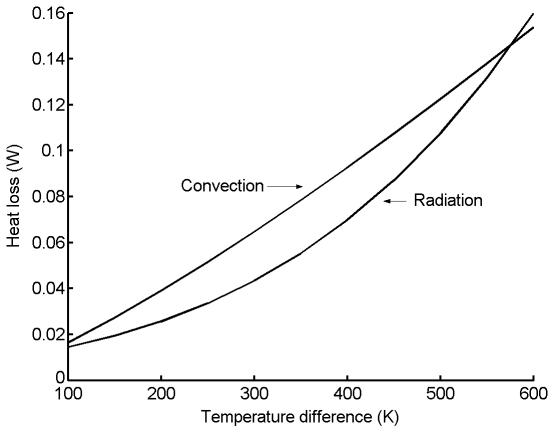

Figure 13. Heat loss versus temperature difference at the film radius of 3 mm.

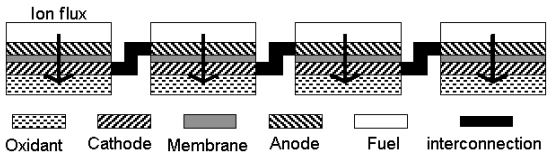

Figure 14. Banded planar interconnection for the fuel cell stack.

4. The plate stack structure of a micro SOFC based on the silicon wafer

A stack of micro solid-oxide fuel cells should be built up to meet the requirement of power and voltage in application. There are two methods to form a planar stack of SOFCs. In conventional planar stacks, cells are configured in a back-to-back orientation, in which bipolar plates are used to separate cells and provide interconnection. Bipolar plates provide short current path and low resistances. But requirements on mechanical and structural integrity are strict to solve cracking problems. Another approach is to arrange the cells with side-by-side configurations in which the cells are connected laterally [4, 18]. Side-by-side configurations are suitable for the micro SOFC cell stack based on microfabrication technologies because all cells can be manufactured in parallel on one wafer in the micromachining processes.

There are two kinds of side-by-side configurations according to the type of interconnection and electrode position. One configuration is shown in figure 14, called a 'banded' configuration. All anodes are on one side of the electrolyte and cathodes on the other side of the electrolyte. Interconnection between neighbouring cells crosses the electrolyte. The advantage is that each of the anodes and cathodes can share one reaction chamber, which may simplify the flow field network for fuel cell stacks. This configuration shows the potential for compact packaging that is important for portable applications. But cell arrays are not suitable for microfabrication based on 2D lithography because interconnection must cross from one side of the wafer to the other side. Another configuration, called a 'flip-flop' design, is shown in figure 15. On each side of the wafer, cathodes and anodes are interlaced. Interconnections do not cross the electrolyte and are short. Single-level interconnection is

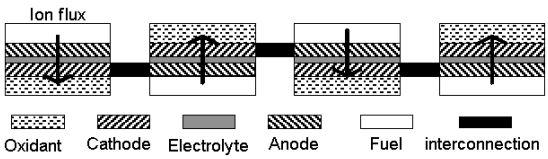

Figure 15. Flip-flop planar interconnection for the fuel cell stack.

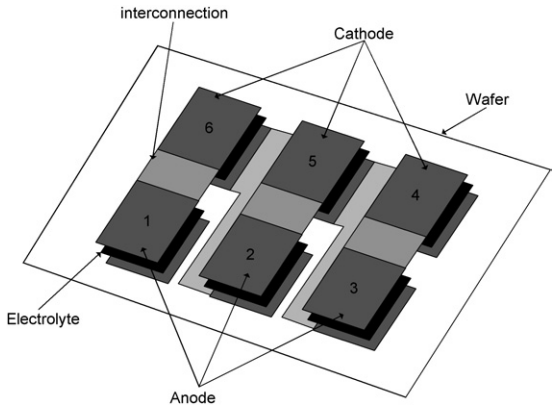

Figure 16. The schematic of lateral configuration of the micro SOFC stack.

advantageous for microfabrication and electrical performance. In this configuration, each cell has an individual reaction chamber. The flow field network is complicated if many cells are integrated in one wafer. Experiments show that some cells in this stack will not achieve their optimal performance. The possible reason is that the flow field in each cell is different [4].

Borrowing the simple flow field network from a banded configuration and the single-level interconnection from a flip-flop configuration, a new flip-flop configuration is presented, as shown in figure 16. On one side of the electrolyte, the two neighbouring electrode columns are different: one column has anodes and the other column has cathodes. The adjacent anodes in one column and cathodes in the other column are connected to build the stack. All cells in the same column share one flow field chamber, which provides a uniform flow field for the cells and the consistent performance of the cells. Compared with the flip-flip design shown in figure 15, such a configuration simplifies the flow field network. Because only adjacent cells are connected, interconnection resistance is low, which is important for a stack with many cells. Sealing is a serious problem in micro SOFCs. Some packaging technologies for MEMS devices, which can withstand high temperature operation, are available [19, 20].

5. Summary

Micro SOFCs with self-supported electrolyte films are one possible choice of portable power sources due to high power density. Thermal–mechanical reliability and heat transfer in thin film micro SOFCs are scale dependent. For a primary optimization design, analytical models are presented for thermal stress, and heat transfer. One novel stack design is also discussed.

Thermal–mechanical reliability is vital in laminated-film SOFCs due to intrinsic stresses in microfabrication and

thermal stresses in operating conditions. Critical stresses in compressive and tensile states for flat and corrugated circular films are analysed. The design diagram shows that corrugated films are more reliable. By taking the advantage of characteristics of stress distribution in the corrugated film, the structure of a flat thin YSZ film with corrugated supported edge is presented to decrease thermal stress in YSZ films.

Analysis of three kinds of heat losses is presented. It shows that air convection and radiation, which increase with the film radius, are the main source of heat loss in large circular thin films with radii of several millimetres. Thermal conduction, which is correlated with film thickness, produces less than 10% of the whole heat loss in large circular thin films. To keep large film area for high performance, optimization of packaging is the primary method to decrease heat loss.

A new flip-flop configuration of the micro SOFC stack is presented. Single-level interconnection simplifies the fabrication of micro SOFCs on one wafer and decreases interconnection resistance. A configuration of the anode column and the cathode column simplifies the flow field network for the micro SOFC stack.

References

[1] Chen X, Wu N J, Smith L and Ignatiev A 2004 Thin-film heterostructure solid oxide fuel cells *Appl. Phys. Lett.* **84** 2700–2

[2] Hertz J L, Lappalanien J and Tuller H L 2002 Progress towards an all thin film fuel cell for portable power generation *Electrochem. Soc. Proc.* **25** 137–45

[3] Singhal S C and Kendall K 2003 *High Temperature Solid Oxide Fuel Cells: Fundamentals, Design and Applications* (Amsterdam: Elsevier)

[4] Lee S J, Chang-Chiem A, Cha S W, Hayre R, Park Y I, Saito Y and Prinz F B 2002 Design and fabrication of a micro fuel cell array with 'flip-flop' interconnection *J. Power Sources* **112** 410–8

[5] Ashby M F 1999 *Materials Selection in Mechanical Design* (Oxford: Butterworth-Heinemann)

[6] Giovanni M Di 1982 *Flat and Corrugated Diaphragm Design Handbook* (New York: Marcel Dekker)

[7] Young W C 1989 *Roark's Formulas for Stress and Strain* (New York: McGraw-Hill)

[8] Haringx A 1957 Design of corrugated diaphragms *Trans. ASME* **79** 54–65

[9] Danzer R 1992 A general strength distribution function for brittle materials *J. Eur. Ceram. Soc.* **10** 461–72

[10] Monstross C S, Yokokawa H and Dokiya M 2002 Thermal stresses in planar solid oxide fuel cells due to thermal expansion difference *Br. Ceram. Trans.* **101** 85–93

[11] Srikar V T, Turner K T, Ie T Y A and Spearing M S 2004 Spearing, structural considerations for micromachined solidoxide fuel cells *J. Power Sources* **125** 62–9

[12] Spiering V L, Bouwstra S, Burger J F and Elwenspoek M 1993 Membranes fabricated with a deep single corrugation for package stress reduction and residual stress relief *J. Micromech. Microeng.* **3** 243–6

[13] Jankowski A F, Hayes J P, Graff R T and Morse J D 2002 Micro-fabricated thin-film fuel cells for portable power requirements *Mater. Res. Soc. Symp. Proc.* **730** 93–8

[14] Incropera F P and Dewitt D P 1996 *Fundamentals of Heat and Mass Transfer* (New York: Wiley)

[15] Sully A H, Brand E A and Waterhouse R B 1952 Some measurements of the total emissivity of metals and pure refractory oxides and the variation of emissivity with temperature *J. Appl. Phys.* **3** 97–101

[16] Hewitt G F, Shires G L and Bott T R 1993 *Process Heat Transfer* (Boca Raton, FL: CRC Press)

[17] Arana L R, Schaevitz S B, Franz A J, Schmidt M A and Jensen L F 2003 A microfabricated suspended-tube chemical reactor for thermally efficient fuel processing *J. Microelectromech. Syst.* **12** 600–12

[18] Gardner F J, Day M J, Brandon N P, Pashley M N and Cassidy M 2000 SOFC technology development at Rolls-Royce *J. Power Sources* **86** 122–9

[19] Mehra A, Ayon A A, Waitz I A and Schmidt M A 1999 Microfabrication of high-temperature silicon devices using wafer bonding and deep reactive ion etching *J. Microelectromech. Syst.* **8** 152–60

[20] An L, Zhang W, Bright V M, Dunn M L and Raj R 2000 Development of injectable polymer-derived ceramics for high temperature MEMS *13th Annual Int. Conf. on Micro Electro Mechanical Systems* (*Miyazaki, Japan*) pp 619–23